JCTC Journal of Chemical Theory and Computation

Article

pubs.acs.org/JCTC

An Efficient N^3-Scaling Propagation Scheme for Simulating Two-Dimensional Infrared and Visible Spectra

Chungwen Liang and Thomas L. C. Jansen*

Zernike Institute for Advanced Materials, University of Groningen, Nijenborgh 4, 9747 AG Groningen, The Netherlands

ABSTRACT: In this paper, we develop and test a new approximate propagation scheme for calculating two-dimensional infrared and visible spectra. The new scheme scales one order more efficiently with the system size than the existing schemes. A Trotter type of approximation is used for the matrix exponent that describes the time evolution of the quantum system. This is needed for calculating the third-order response functions governing the two-dimensional infrared and visible spectra. The method is tested on a model dimer system, the amide I spectrum of the Gramicidin A antimicrobial peptide, the spectrum of the OH stretching vibration of bulk water, and a homogeneous J-aggregate. Errors due to the approximation are hardly observable in the calculated spectra. Scaling simulations with different system sizes are used to demonstrate that the new scheme is indeed scaling with the system size to the third power, one order faster than the existing methods.

1. INTRODUCTION

Two-dimensional spectroscopy has become a popular tool to study diverse phenomena, from structure and dynamics in peptides[1−5] and DNA[6] to exciton motion in light harvesting complexes.[7] The systems of interest are often very complex, and the spectra are far from straightforward to interpret. Therefore, high level theory is needed. The spectral simulations are, however, also very time-consuming. Efficient calculation schemes are therefore needed. In this paper, we will present an approximate scheme that provides accurate results at small computational cost given that a Hamiltonian trajectory (i.e., the time-dependent parameters describing the quantum system under consideration) is already known.

Many efforts have been made to allow the simulation of two-dimensional spectra of extensive systems.[8−26] The static sum-overstates method based on diagonalizing the Hamiltonian and calculating the two-dimensional spectrum in the frequency domain is limited by the need of diagonalizing the two-exciton part of the Hamiltonian, which scales as N^6, where N is the number of coupled sites. When only a part of the total spectrum is desired, as the region around the super radiant state of a J-aggregate, diagonalization schemes only providing the low energy states contribution to the spectrum can be applied.[8,27] Using the Nonlinear Exciton Equation (NEE) formulation,[9] the two-exciton Hamiltonian diagonalization is reformulated into a scattering problem, circumventing the diagonalization of the two-exciton Hamiltonian and resulting in the N^4 scaling NEE approach. However, these static schemes neglect the effect of fast bath fluctuations on the spectra. The time-averaging approximation approach, which replaces the instantaneous Hamiltonian with a time-averaged one, can be used to account for the effect of these fluctuations,[10,11] at least to some extent. Recently, a promising version of this approximation that accurately describes the linear absorption of bulk water was presented.[12]

The bath fluctuations can be accounted for in the mixed quantum-classical approaches that are based on calculating the third-order response function in the time domain and then Fourier transforming to the frequency domain. These methods at first sight do not offer an improvement, as the two-exciton Hamiltonian still needs to be diagonalized for the propagation during the probe coherence time. The Numerical Integration of the Schrödinger Equation (NISE) scheme[13,14] relying on this method allowed the simulation of the amide I region 2DIR spectrum of Trpzip2, a β-sheet peptide with 12 coupled amide I units.[15] The application of the combination of Wick's theorem and the Trotter formula for the propagation assuming that the anharmonicity can be treated as a small perturbation of the harmonic Hamiltonian allowed for application to a 128 coupled oscillator system.[16] In this scheme, the propagation of the two-exciton states scales as N^4. The approach was further refined by reformulating it in the NEE framework[17] and by applying a sparse matrix approach.[18] The latter allows a limiting scaling behavior of N^3, as all couplings go to zero. In this paper, we will present an approximate propagation scheme that reduces the scaling behavior to N^3 for coupled systems and to just N^2 when the Hamiltonian is sparse.

In the present approach, the system is treated quantum mechanically, and the bath is treated classically.[28] This approximation is only valid when the temperature is large compared to the bandwidth of the spectrum, which is usually valid for infrared spectra at room temperature. However, it becomes more dubious for visible spectra and at temperatures much below room temperature. If these conditions are not fulfilled, one may apply the hierarchy equations of motion approach,[26,29] which treats the bath degrees of freedom quantum mechanically, but it is more computationally costly than the approach discussed here. In the case of a strong coupling with the

Received: January 25, 2012
Published: March 29, 2012

dx.doi.org/10.1021/ct300045c | J. Chem. Theory Comput. 2012, 8, 1706−1713

surroundings, the mixed quantum-classical Liouville approach[30,31] may be more appropriate to apply, which again is more time costly than the approach considered here. Finally, for low frequency modes that can be considered to be fully classical, nonequilibrium molecular dynamics approaches have been applied[32−34] for calculating nonlinear response functions.

The outline of the reminder of this paper is as follows. In the following section, we will first discuss the theory behind the new approximate propagation scheme. In section 3, we will apply the scheme to four different systems to demonstrate how well it works. Finally, in the last section, we will draw our conclusions.

2. THEORY

The quantum-classical response functions describe linear absorption and nonlinear response as the two-dimensional spectra depend on the transition dipoles between the involved quantum mechanical states, the Newtonian evolution of the classical system, and the quantum evolution of the spectroscopic important states.[28,35,36] The typical Hamiltonian used to model the first- and third-order response functions governing these spectroscopic measurements is

$$H(\vec{R}) = \sum_{i}^{N} \omega_i(\vec{R})\, B_i^{\dagger} B_i + \sum_{i,j}^{N} J_{ij}(\vec{R})\, B_i^{\dagger} B_j - \sum_{i}^{N} \frac{\Delta_i(\vec{R})}{2} B_i^{\dagger} B_i^{\dagger} B_i B_i + \sum_{i}^{N} \vec{E}\cdot\vec{\mu}_i(\vec{R})\,(B_i^{\dagger} + B_i) \tag{1}$$

The Hamiltonian parameters may depend on the classical bath cooridinates ($\vec{R}$). The indices i and j run over the N sites. $B_i^{\dagger}$ and B_i are the Bosonic creation and annihilation operators. The site frequencies are ω_i, the couplings J_{ij}, and the anharmonicities Δ_i. The coupling with the external electric laser field $\vec{E}$ is determined by the transition dipole moments $\vec{\mu}_i$. In this Hamiltonian, all terms but the last conserve the number of excitations. Only when an external electric field is present are transitions from the ground state to the single excitation manifold or transitions from the single excitation manifold to the double excitation manifold possible.

The Newtonian equations of motion that describe the bath dynamics are either solved with the Euler method[37] or the procedures implemented in the molecular dynamics (MD) program GROMACS.[38] It is assumed that the bath dynamics is independent of the state of the quantum degrees of freedom.[36] The dynamics of the quantum system is determined by the time-dependent Schrödinger equation. This equation is solved by dividing time into small intervals, assuming that the Hamiltonian is constant during each interval, and then solving the time-independent Schrödinger equation for each interval. The formal solution for each time interval is expressed in terms of the time-evolution operator:

$$U(t + \Delta t, t) = \exp\left(-\frac{i}{\hbar} H(\vec{R}(t))\Delta t\right) \tag{2}$$

Which means that the wave function at time $t + \Delta t$ is

$$\phi(t + \Delta t) = U(t + \Delta t, t)\, \phi(t) \tag{3}$$

In practice, the problem is solved independently on the basis of the single excitation manifold and the double excitation manifold, as those do not couple, when no external electric field is present. There are N single excited states and $N(N + 1)/2$ double excited states. Equation 2 can be solved by diagonalizing the Hamiltonian in the matrix representation, taking the exponent of the eigenvalues and transforming back to the site basis. This was how the nonlinear response functions were originally solved.[13] Numerous other propagation schemes have been suggested in the literature.[37,39,40] The problem can be solved approximately using the Trotter formula

$$\exp(A + B) = \exp(A/2)\exp(B)\exp(A/2) + \ldots \tag{4}$$

where A and B are different parts of the Hamiltonian matrix and the higher-order terms of the expansion are neglected. This was utilized to speed up the calculation of the double excitation manifold by splitting the Hamiltonian into a harmonic and an anharmonic part.[16] The solution to the harmonic part can be given by a combination of the time-evolution matrices for the single excitation manifold, and the anharmonic part, which is either sparse[16] or diagonal.[18] This reduces the cost for calculating the time-evolution operator for the double excitation manifold from N^6 to N^4. The calculation cost for the single excitation manifold remains at N^3. Using sparse techniques, the cost for propagating the double excitation manifold can be reduced to N^3 in the limit where the coupling between the sites becomes negligible.[18]

Here, we approximate the time-evolution operator by the expansion

$$\exp(A_0 + \sum_{i,j} A_{ij}) = \exp(A_0/2)\Big[\prod_{i,j,k} \exp(A_{ijk})\Big] \times \exp(A_0/2) + \ldots \tag{5}$$

where A_0 is the diagonal part of the Hamiltonian including the fundamental frequencies and, for the double excitation manifold, the anharmonicities.

$$A_0 = -\frac{i}{\hbar}\left(\sum_{i}^{N} \omega_i(\vec{R})\, B_i^{\dagger} B_i - \sum_{i}^{N} \frac{\Delta_i(\vec{R})}{2} B_i^{\dagger} B_i^{\dagger} B_i B_i\right) \tag{6}$$

The terms A_{ijk} are given by the couplings using the following expressions

$$A_{ijk} = -\frac{i}{\hbar} J_{ij}(\vec{R})\, B_i^{\dagger} B_j\, \delta_{ik}(1 - \delta_{ij}) \tag{7}$$

$$A_{ijk} = -\frac{i}{\hbar} J_{ij}(\vec{R})\, B_i^{\dagger} B_k^{\dagger} B_k B_j \frac{(1 - \delta_{ij})}{\sqrt{1 + \delta_{ik} + \delta_{jk}}} \tag{8}$$

for the single excitation and double excitation manifolds, respectively. The expressions for the two cases are different, so eq 5 is the same for the single and double excitation manifolds. For the single excitation manifold, each A_{ijk} with $k = i$ results in the coupling of a pair of site basis functions, while each A_{ijk} for the double excitation manifold results in the coupling of a pair of site basis functions, and the term $(1 + \delta_{ik} + \delta_{jk})^{1/2}$ ensures the correct normalization.

This reduces the computational cost of propagating the single excitation manifold to $N(N + 1)/2$, because we need

to loop over the couplings and the site frequencies. For the double excitation manifold, the propagation scales as $N^2(N+1)/2$, because the Hamiltonian does not couple double excited states that are different in more than one of the two excitations. The matrices A_{ijk} all contain only two off-diagonal elements and are trivial to diagonalize, resulting in a trivial expression for the matrix elements of $\exp(A_{ijk})$:

$$\langle i|\exp(A_{ijk})|j\rangle = -i\,\sin(\Delta t J_{ij}/\hbar)\,\delta_{ik}(1-\delta_{ij}) \tag{9}$$

$$\langle i|\exp(A_{ijk})|i\rangle = \cos(\Delta t J_{ij}/\hbar)\,\delta_{ik}(1-\delta_{ij}) \tag{10}$$

$$\langle ik|\exp(A_{ijk})|jk\rangle = -i\,\sin(\Delta t\sqrt{1+\delta_{ik}+\delta_{jk}}J_{ij}/\hbar)(1-\delta_{ij}) \tag{11}$$

$$\langle ik|\exp(A_{ijk})|ik\rangle = \cos(\Delta t\sqrt{1+\delta_{ik}+\delta_{jk}}J_{ij}/\hbar)(1-\delta_{ij}) \tag{12}$$

and the corresponding hermitian conjugates. All other diagonal elements are one, and off-diagonal elements are zero. In the following, we will distinguish between propagation in the two excitation manifolds with U^{ee} and U^{ff} denoting propagation in the single excited and double excited state manifolds, respectively. Likewise, we will denote a transition dipole vector taking the system from the ground state to the single excited state manifold μ^{eg} and a transition dipole matrix taking the system from the single excited state manifold to the double excited state manifold μ^{fe}.

This is then used in the expressions for the response functions. The linear absorption is given by the Fourier transform of the two-point correlation function of the transition dipole:

$$I(\omega) = \mathrm{Im}\int_0^\infty \mathrm{d}t_1 \frac{i}{\hbar}\langle \mu^{ge}(\tau_2)\,U^{ee}(\tau_2,\tau_1)\,\mu^{eg}(\tau_1)\rangle \times \exp(-i\omega t_1)\,\Gamma_{\mathrm{LA}}(t_1) \tag{13}$$

Here, τ_2 and τ_1 are the times, when the system interacts with the external field and t_1 is the time between these interactions ($t_1 = \tau_2 - \tau_1$). Here and hereafter, $\langle ... \rangle$ denotes the ensemble average, which is obtained by summing over the contributions from configurations at different starting points along the classical trajectory. The vibrational lifetime is accounted for by the *ad hoc* relaxation factor:

$$\Gamma_{\mathrm{LA}}(t_1) = \exp(-t_1/2T_1) \tag{14}$$

where T_1 is the lifetime of the single excited states. The subscript LA indicates that this is for the linear absorption.

The 2DIR spectrum is given as the sum of the signal emitted in the directions with wave vectors $\bar{k}_{\mathrm{I}} = -\bar{k}_1 + \bar{k}_2 + \bar{k}_3$ and $\bar{k}_{\mathrm{II}} = \bar{k}_1 - \bar{k}_2 + \bar{k}_3$, where $\bar{k}_1$, $\bar{k}_2$, and $\bar{k}_3$ are the wave vectors of the incoming infrared fields. $\bar{k}_{\mathrm{I}}$ is the photon-echo signal, and $\bar{k}_{\mathrm{II}}$ is the nonrephasing signal. Each of these signals contains three contributions from distinct Liouville space pathways: ground state bleach (GB), stimulated emission (SE), and excited state absorption (EA).[28,41] These are given by

$$\begin{aligned}
S^{(\mathrm{I})}_{\mathrm{GB}}(t_3,t_2,t_1) &= -\left(\frac{i}{\hbar}\right)^3\langle \mu^{ge}(\tau_1)\,U^{ee}(\tau_1,\tau_2)\,\mu^{eg}(\tau_2)\,\mu^{ge}(\tau_4) \times U^{ee}(\tau_4,\tau_3)\,\mu^{eg}(\tau_3)\rangle\\
S^{(\mathrm{I})}_{\mathrm{SE}}(t_3,t_2,t_1) &= -\left(\frac{i}{\hbar}\right)^3\langle \mu^{ge}(\tau_1)\,U^{ee}(\tau_1,\tau_2)\,U^{ee}_{\mathrm{exp}}(\tau_2,\tau_3) \times \mu^{eg}(\tau_3)\,\mu^{ge}(\tau_4)\,U^{ee}(\tau_4,\tau_3)\,U^{ee}_{\mathrm{exp}}(\tau_3,\tau_2) \times \mu^{eg}(\tau_2)\rangle\\
S^{(\mathrm{I})}_{\mathrm{EA}}(t_3,t_2,t_1) &= \left(\frac{i}{\hbar}\right)^3\langle \mu^{ge}(\tau_1)\,U^{ee}(\tau_1,\tau_2)\,U^{ee}_{\mathrm{exp}}(\tau_2,\tau_3) \times U^{ee}(\tau_3,\tau_4)\,\mu^{ef}(\tau_4)\,U^{ff}(\tau_4,\tau_3)\,\mu^{fe}(\tau_3) \times U^{ee}_{\mathrm{exp}}(\tau_3,\tau_2)\,\mu^{eg}(\tau_2)\rangle\\
S^{(\mathrm{II})}_{\mathrm{GB}}(t_3,t_2,t_1) &= -\left(\frac{i}{\hbar}\right)^3\langle \mu^{ge}(\tau_4)\,U^{ee}(\tau_4,\tau_3) \times \mu^{eg}(\tau_3)\,\mu^{ge}(\tau_2)\,U^{ee}(\tau_2,\tau_1)\,\mu^{eg}(\tau_1)\rangle\\
S^{(\mathrm{II})}_{\mathrm{SE}}(t_3,t_2,t_1) &= -\left(\frac{i}{\hbar}\right)^3\langle \mu^{ge}(\tau_2)\,U^{ee}_{\mathrm{exp}}(\tau_2,\tau_3) \times \mu^{eg}(\tau_3)\,\mu^{ge}(\tau_4)\,U^{ee}(\tau_4,\tau_3)\,U^{ee}_{\mathrm{exp}}(\tau_3,\tau_2) \times U^{ee}(\tau_2,\tau_1)\,\mu^{eg}(\tau_1)\rangle\\
S^{(\mathrm{II})}_{\mathrm{EA}}(t_3,t_2,t_1) &= \left(\frac{i}{\hbar}\right)^3\langle \mu^{ge}(\tau_2)\,U^{ee}_{\mathrm{exp}}(\tau_2,\tau_3)\,U^{ee}(\tau_3,\tau_4) \times \mu^{ef}(\tau_4)\,U^{ff}(\tau_4,\tau_3)\,\mu^{fe}(\tau_3)\,U^{ee}_{\mathrm{exp}}(\tau_3,\tau_2) \times U^{ee}(\tau_2,\tau_1)\,\mu^{eg}(\tau_1)\rangle
\end{aligned} \tag{15}$$

τ_1 through τ_4 are the times for interactions with the external electric field, and t_1 through t_3 are the time delays between these (i.e., $t_1 = \tau_2 - \tau_1$, $t_2 = \tau_3 - \tau_2$, and $t_3 = \tau_4 - \tau_3$). During the waiting time, t_2, the more accurate propagation using the full matrix exponent given in eq 2 is used; this time-evolution matrix is denoted $U^{ee}_{\mathrm{exp}}(\tau_3,\tau_2)$ in the expression above. This matrix is used because the waiting time can be extended to much longer times than the coherence times t_1 and t_3. We want to be able to describe that dynamics as accurate as possible. At the same time, the system is never in a double excited state during the waiting time, and the propagation with $U^{ee}_{\mathrm{exp}}(\tau_3,\tau_2)$ scales as N^3 when we use the full matrix exponential.

The vibrational lifetime is included in an *ad hoc* way through the relaxation factor

$$\Gamma(t_3,t_2,t_1) = \exp(-(t_3+2t_2+t_1)/2T_1) \tag{16}$$

We multiply all third-order response functions with this factor. Note that since we do not describe relaxation between the excitation manifolds through the Hamiltonian, it is not possible to correctly model more complex decay to the ground state, which is simply taken to be exponential here. The decay of the ground state bleach in this *ad hoc* model arises from cancellation with contributions from the decayed stimulated emission and excited state absorption.

The signals are converted to the frequency domain using 2D Fourier transforms with respect to the coherence times t_1 and t_3:

$$S^{(\mathrm{I})}(\omega_3, t_2, \omega_1) = \int_0^\infty \int_0^\infty (S^{(\mathrm{I})}_{\mathrm{GB}}(t_3, t_2, t_1) + S^{(\mathrm{I})}_{\mathrm{SE}}(t_3, t_2, t_1) + S^{(\mathrm{I})}_{\mathrm{EA}}(t_3, t_2, t_1)) \times \exp(i(\omega_3 t_3 - \omega_1 t_1))\, \mathrm{d}t_3\, \mathrm{d}t_1$$

$$S^{(\mathrm{II})}(\omega_3, t_2, \omega_1) = \int_0^\infty \int_0^\infty (S^{(\mathrm{II})}_{\mathrm{GB}}(t_3, t_2, t_1) + S^{(\mathrm{II})}_{\mathrm{SE}}(t_3, t_2, t_1) + S^{(\mathrm{II})}_{\mathrm{EA}}(t_3, t_2, t_1)) \times \exp(i(\omega_3 t_3 + \omega_1 t_1))\, \mathrm{d}t_3\, \mathrm{d}t_1 \quad (17)$$

Finally, the 2DIR correlation spectrum is the imaginary part of the sum of the photon-echo and nonrephasing signals:

$$I_{2\mathrm{D}}(w_3, t_2, w_1) = \mathrm{Im}(S^{(\mathrm{I})}(w_3, t_2, w_1) + S^{(\mathrm{II})}(w_3, t_2, w_1)) \quad (18)$$

The parallel and perpendicular polarization spectra are obtained using the proper averaging over polarization components of the transition dipole vectors as described elsewhere.[42,43] This involves averaging over 21 different polarization directions in the simulation coordinate frame for each starting point.

3. RESULTS AND DISCUSSION

3.1. Dimer Model. We first tested the method on a model dimer system. We created a trajectory of a fluctuating Hamiltonian of 1 ns length with snapshots stored every 10 fs. The frequencies were constructed so that they fluctuate with a standard deviation of 10 cm^{-1} and a correlation time of 1 ps. The frequencies of the two sites were constructed so that they are uncorrelated with each other. The average frequencies of the two sites are 1495 and 1505 cm^{-1}, and a fixed coupling of 25 cm^{-1} was imposed. The angle between the transition dipoles of the two sites was set to 90°. For the coherence times, a maximum of 2.56 ps was used, and the waiting time was set to 0 fs. The resulting linear absorption spectra are shown in Figure 1, and the 2DIR spectra with parallel polarization are

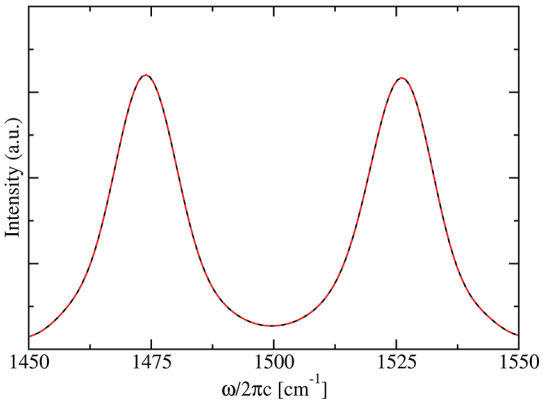

Figure 1. The linear absorption spectrum of the dimer model with the matrix exponent propagation method (dashed black) and with the new propagation scheme (dashed red).

shown in Figure 2. Only by zooming in very closely on the linear absorption spectra is a numerical difference observed between the full matrix exponent propagation scheme and the new one. The 2DIR spectra are also essentially identical. With the original scheme, the calculation of the 2DIR spectrum took 1615 s, while it took 760 s with the new scheme, when

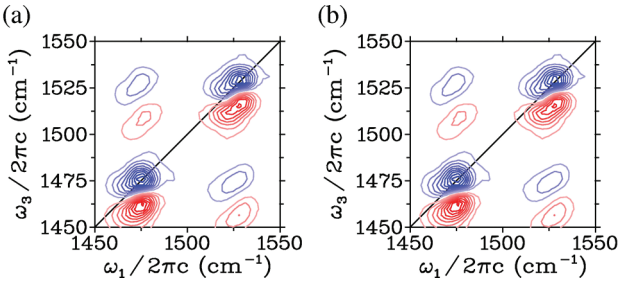

Figure 2. The parallel polarization 2DIR spectrum of the dimer model with the matrix exponent propagation method (a) and with the new propagation scheme (b). Equidistant contour lines are drawn. Blue lines represent the bleach signal, and red lines represent the excited state absorption signal.

averaging over 95 starting points along the trajectory (on a 3.06 GHz Intel Core 2 Duo iMac). The new scheme is thus about twice as fast as the full matrix exponent scheme.

3.2. Gramicidin A. Gramicidin A is a dimer peptide produced by natural bacteria acting as an antibiotic. We used a Hamiltonian trajectory for the amide I band from a previous study.[44] The trajectory started with the helical dimer structure from the protein data bank (PDB: 1JNO,[45] see Figure 3a) and

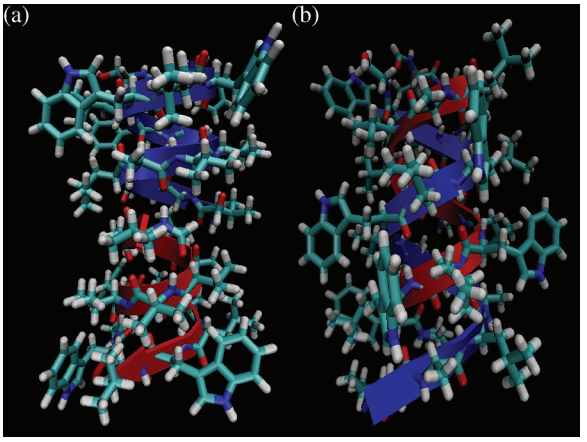

Figure 3. The structures of the helical dimer (a) and the double helix (b) conformation of Gramicidin A drawn with VMD (ref 51). The backbones of the two chains are drawn in blue and red.

is 10-ns-long with 20 fs between each snapshot. The Hamilton was constructed by combining a MD trajectory with a mapping procedure to obtain the amide I frequencies and couplings.[43,46] The dimer peptide has 32 amide I vibrations. The parallel polarization two-dimensional spectra for the amide I region were simulated using coherence times up to 2.56 ps and a waiting time of 0 fs. Samples were calculated with 100 ps between each sample point, resulting in 100 samples. The linear absorption and 2DIR spectra are presented in Figures 4 and 5, respectively. Differences between the spectra obtained with the full exponential propagation and the new propagation method are hardly visible. The calculation took 16 000 min with the full matrix exponent propagation and only 450 min with our new propagation scheme, equivalent to a speed-up factor of 35 (on a 2.80 GHz Intel Core i7 CPU running linux).

Gramicidin A is known to exist in a double helix conformation as well (PDB: 1AV2,[47] see Figure 3b). We used the same procedure as for the helical dimer to calculate the linear and 2DIR spectrum of this conformation as shown in

dx.doi.org/10.1021/ct300045c | J. Chem. Theory Comput. 2012, 8, 1706−1713

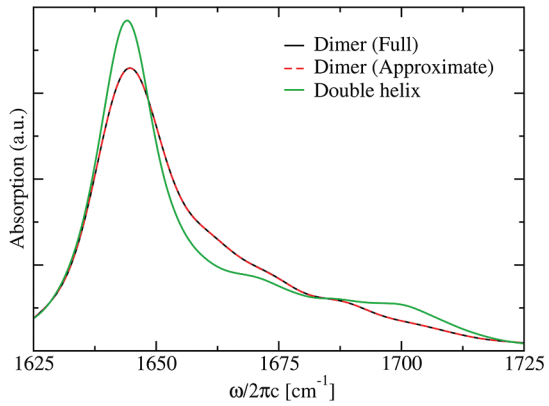

Figure 4. The linear absorption spectrum of the helical dimer conformation of Gramicidin A obtained with the sparse propagation method (black) and with the new propagation scheme (red). The linear absorption spectrum of the double helix conformation of Gramicidin A with the new propagation scheme.

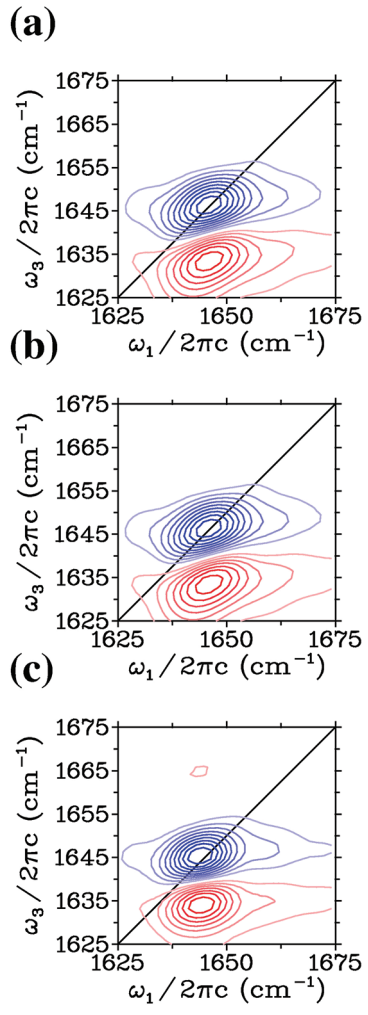

Figure 5. The parallel polarization 2DIR spectrum of the helical dimer conformation of Gramicidin A obtained with the sparse propagation method (a) and with the new propagation scheme (b). (c) The parallel polarization 2DIR spectrum of the double helix conformation of Gramicidin A with the new propagation scheme. The contour lines are plotted with the same convention as in Figure 2.

Figures 4 and 5, respectively. The spectra for this conformation of Gramicidin A have similar features as those seen for the helical dimer; however, the spectra are still clearly distinguishable. The main peak of the double helix conformation is narrower than that of the helical dimer.

3.3. Liquid Water. Liquid water has been a testing ground for most of the recently developed schemes for simulating 2DIR spectra.[10,12,16−18] We applied our new method to the same Hamiltonian as used in ref 18 and with identical settings for the calculation with the exception of the propagation scheme. The simulation box contained 128 coupled OH stretch vibrations. The time step used for the propagation scheme was 10 fs. For $t_2 = 0$, the new method takes 22.5 CPU hours for 100 samples, whereas the calculation with the sparse matrix propagation scheme took 3500 CPU hours[18] (on a single core of a Six-Core AMD Opteron Processor 2435 running linux). This corresponds to a speed-up factor of 150. The 2DIR spectra for both parallel and perpendicular polarizations are presented in Figure 6. Again, essentially no difference is

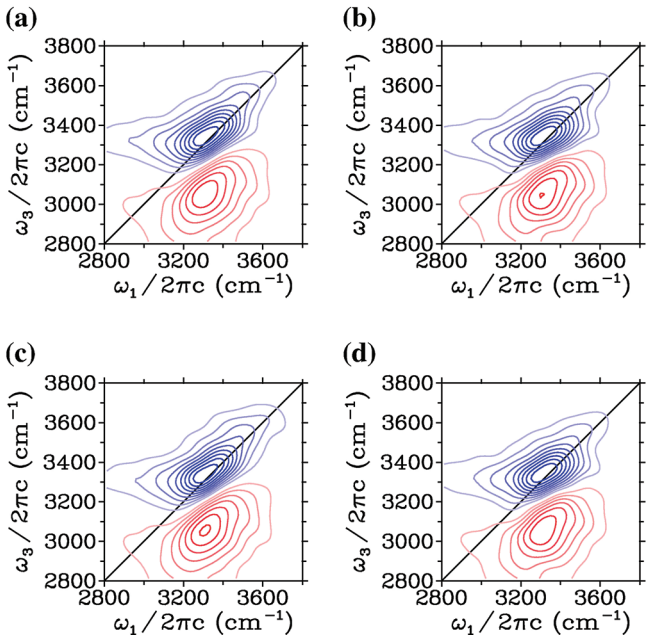

Figure 6. The 2DIR spectrum of water obtained with the sparse propagation method (a and b) and with the new one (c and d) for the parallel and perpendicular polarization, respectively. The contour lines are plotted with the same convention as in Figure 2.

observed in the calculated spectra with the two methods. In Figure 7, the spectra integrated over ω_1 corresponding to a pump probe experiment with a broad pump and a narrow probe is given. Here, a slight difference in the peak positions is observed between the new propagation scheme and the sparse scheme.

3.4. J-Aggregate. The biggest challenge for the new propagation scheme is when the excitations are highly delocalized. In homogeneous J-aggregates, the excitations are fully delocalized over all molecules in the aggregate. We applied the new approach to the calculation of the linear spectrum of a homogeneous aggregate with 25 sites. We assume that the aggregate is linear and that there is only a coupling between nearest neighbors of value −600 cm^{-1}. All sites are assumed to have the same constant frequency of 12 000 cm^{-1} and parallel transition dipoles. An excitation lifetime of 1 ps is applied. The spectra were calculated for different values of the time step. As the couplings in this case are much larger than those found between amide I vibrations of peptides and OH stretch

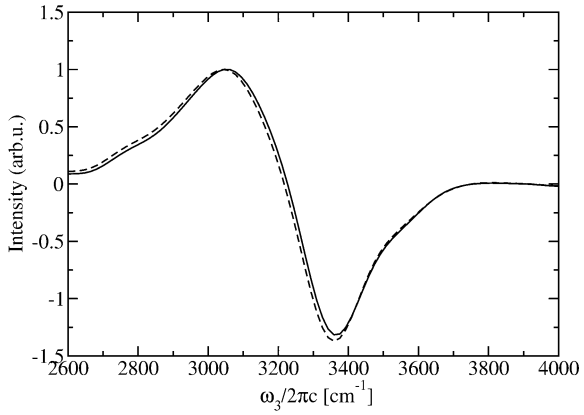

Figure 7. The broad pump narrow probe signal obtained from integrating the parallel polarization 2DIR spectra over ω_1 for the new propagation scheme (solid line) and the sparse propagation scheme (dashed line).

vibrations of water, the time steps needed are smaller as well. In Figure 8, the spectra are shown calculated with time steps of

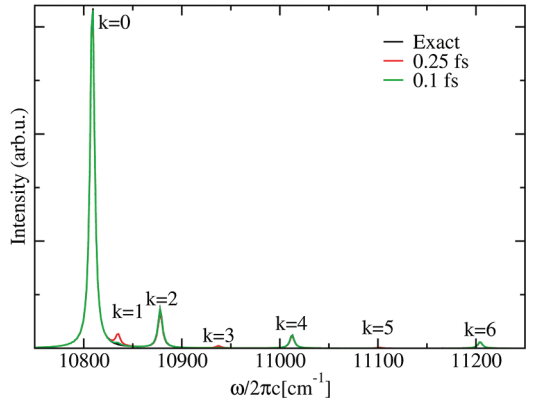

Figure 8. The linear absorption spectrum of a homogeneous J-aggregate using different time step sizes in the propagation. The peaks are labeled by the number of the corresponding eigenstate.

0.1 fs and 0.25 fs as well as with the exact matrix exponent scheme using a time step of 5 fs. Peaks are observed for the seven lowest eigenstates numbered from k = 0 to 6. By symmetry, the odd numbered eigenstates should be prohibited. It is seen that for time steps of 0.25 fs, this is not obeyed by the simulation. For 0.1 fs time steps, the selection rule violation can hardly be discerned.

The two-dimensional optical spectrum was calculated using an artificial anharmonicity of 4000 cm^{-1} to eliminate double excited states on the same site.[48,49] The coherence times were accounted for up to 10 ps. The waiting time was fixed at zero. An excitation lifetime of 0.9 ps was employed to match previous simulations.[8] The calculated spectrum is very similar to that of ref 8, which used the sum-overstates method for the spectral calculation as shown in Figure 9. Minor differences in the peak positions are seen. This can be a result of the fact that the unphysical double excited states on the same site were included in the present simulation but not the original sum-overstates one. When only looping over the nonzero elements of the Hamiltonian during the propagation, the present calculation took 87 h (on a single core of a Six-Core AMD Opteron Processor 2435 running linux). The long duration arises from the fact that narrow lines are calculated (i.e., high resolution is needed) in a broad

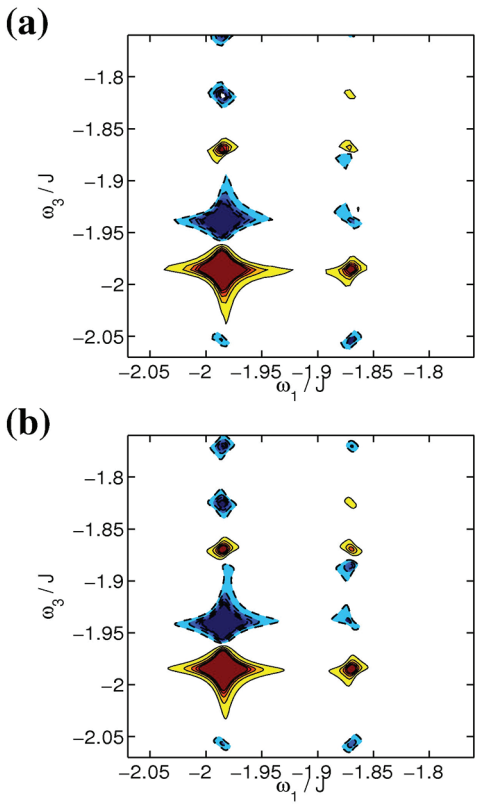

Figure 9. The simulated two-dimensional optical spectrum of a homogeneous J-aggregate with the new propagation method (a) and with the sum-over-states method (b) (reproduced from ref 8). The contours are drawn at 1% intervals between −5% and +5% of the maximum intensity. The bleach signals are colored in red, while excited state absorption is blue.

spectrum. The time steps thus need to be short, and at the same time, the coherence times need to be calculated to significantly longer times than the excitation lifetime to obtain a nice spectrum. If one simulates spectra with disorder, the peaks will become broader, and one may reduce the length of the calculated coherence time, resulting in shorter calculation times.

3.5. Scaling Behavior. The scaling behavior was tested by selecting random subensembles of the water Hamiltonian trajectory. This can also be thought of as diluting the water with heavy water, resulting in a mixture of D_2O, HOD, and H_2O. We created Hamiltonian trajectories with 8, 16, 32, 64, and 128 oscillators and simulated the spectra with identical settings as in the subsection 3.3. The CPU times were recorded (see Figure 10) and fitted with a polynomium $t = \alpha N^{\beta}$, where t is the CPU time in seconds, N is the number of oscillators, and α and β are a prefactor and the scaling exponent, respectively. These parameters were found to be 0.22 CPU seconds and 2.7, respectively. The deviation of the latter number from 3 indicates that other parts of the calculation scaling faster than N^3 contribute significantly to the total calculation time. For example, reading the Hamiltonian from a disk, propagating the single excitation wave functions, and multiplying with the transitions dipoles μ^{ef} are all expected to scale as N^2.

For the J-aggregates, where only nearest neighbor interactions were included, this was used to make the scheme sparse by only looping over nonzero coupling elements in the propagation routine. This resulted in calculation times of 15.5, 86.75, and 172.25 h for aggregate lengths of 10, 25, and 35, respectively. A fit

dx.doi.org/10.1021/ct300045c | J. Chem. Theory Comput. 2012, 8, 1706−1713

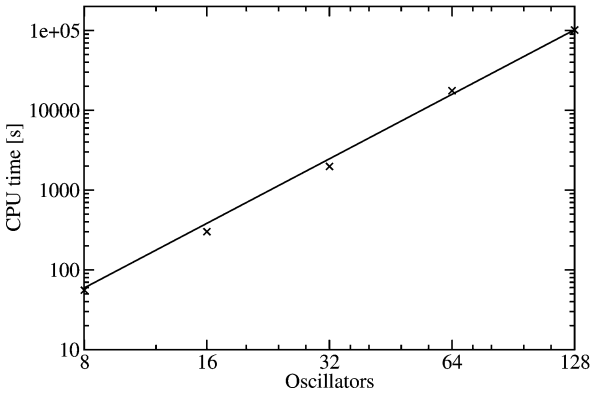

Figure 10. A double log representation of the scaling behavior of the new propagation scheme obtained for different numbers of water OH stretch oscillators. Crosses are data points; the black line is a polynomial fit.

shows that this corresponds to N^2 scaling. For sparse Hamiltonians, the propagation scheme is thus even more efficient that the N^3 applying to general systems.

3.6. Discussion. The new propagation scheme is expected to be valid as long as the couplings are not too strong (terms like $J_{ij}J_{jk}\Delta t^2/\hbar^2$ and $J_{ij}(\omega_i - \omega_j)\Delta t^2/\hbar^2$ must be small). It was demonstrated that on realistic vibrational systems the approximation is hardly visible, when Δt is 10−20 fs. One can expect J-aggregates to be a worst case scenario for the present approximation because the excitations are completely delocalized. For those systems, time steps of 0.1 fs were small enough to practically eliminate observable effects of the approximation. For future applications, the validity will still need to be tested, in particular, when the couplings are larger than in the systems treated here. As the error scales with the size of the time step, the convergence of the approximation can be tested simply by comparing simulations with different time steps, as was done here for the homogeneous J-aggregate.

In this paper, we did not vary the waiting time t_2. We propose treating dynamics during this time without approximation as this for t_2 scales as N^3. If very long waiting times are used, the time spent on this part of the calculation will become significant. Still the scaling will be as N^3. One could apply the approximate scheme for waiting time dynamics as well to get N^2 scaling for the t_2 part of the calculation; one should then carefully verify that this does not affect the observed waiting time dynamics.

The present approach does not allow the inclusion of coupling between the excitation manifolds. This cannot be correctly done without including the effect of the excitation on the dynamics of the bath. Including relaxation and quantum state dependent bath dynamics needs to be considered carefully if one needs to account for these effects. Depending on the approach that one takes for such treatment, the approximation introduced here might be useful. For example, if using a Liouville equation based approach, similar exponentials to those found here appear. When including multiple excitation manifolds at the same time, one should, however, be aware that much shorter time steps will be needed, as these should be shorter than $\hbar$ divided by the energy difference between the lowest and highest energy states.

4. CONCLUSIONS

In this paper, we presented a new propagation scheme for calculating first- and third-order response functions in the quantum-classical approximation. The new propagation scheme is based on a Trotter type expansion of the time-evolution operator that avoids the costly diagonalization of the Hamiltonian for the double excited states needed in the calculation of the third-order response functions. The new propagation scheme was implemented in the existing NISE2A program[50] and tested on a dimer, the Gramicidin A antimicrobial peptide, bulk water, and a homogeneous J-aggregate. We found that with the new propagation scheme, the calculations are about N times faster than with the sparse matrix exponent[18] and propagation of the nonlinear exciton equations schemes.[17] In practice, it scales approximately as N^3 and as N^2 when the Hamiltonian is sufficiently sparse. The new propagation scheme will extend the regime of systems for which the two-dimensional spectra can be calculated. For example, it is now possible to simulate spectra of proteins of higher relevance to biology than was possible before. Furthermore, the propagation scheme is likely to be applicable to solving time-dependent Schrödinger and Liouville equations in many other fields of theoretical chemistry and physics.

AUTHOR INFORMATION

Corresponding Author

*E-mail: T.L.C.Jansen@rug.nl.

Notes

The authors declare no competing financial interest.

ACKNOWLEDGMENTS

T.L.C.J. acknowledges The Netherlands Organization for Scientific Research (NWO) for support through a VIDI grant. Erik Bloemsma is gratefully acknowledged for helpful discussions and Arend Dijkstra for sharing his raw data for the homogeneous J-aggregate and for suggesting to add the comparison between the broad pump−narrow probe representation of the 2DIR data for water.

REFERENCES

(1) Hamm, P.; Lim, M. H.; Hochstrasser, R. M. *J. Phys. Chem. B* **1998**, *102*, 6123.
(2) Woutersen, S.; Hamm, P. *J. Chem. Phys.* **2001**, *115*, 7737.
(3) Cheatum, C. M.; Tokmakoff, A.; Knoester, J. *J. Chem. Phys.* **2004**, *120*, 8201.
(4) Maekawa, H.; Toniolo, C.; Moretto, A.; Broxterman, Q. B.; Ge, N.-H. *J. Phys. Chem. B* **2006**, *110*, 5835.
(5) Manor, J.; Mukherjee, P.; Lin, Y.-S.; Leonov, H.; Skinner, J. L.; Zanni, M. T.; Arkin, I. T. *Structure* **2009**, *17*, 247.
(6) Krummel, A. T.; Mukherjee, P.; Zanni, M. T. *J. Phys. Chem. B* **2003**, *107*, 9165−9169.
(7) Brixner, T.; Stenger, J.; Vaswani, H. M.; Cho, M.; Blankenship, R. E.; Fleming, G. R. *Nature* **2005**, *434*, 625.
(8) Dijkstra, A. G.; Jansen, T. L. C.; Knoester, J. *J. Chem. Phys.* **2008**, *128*, 164511.
(9) Mukamel, S.; Abramavicius, D. *Chem. Rev.* **2004**, *104*, 2073.
(10) Auer, B. M.; Skinner, J. L. *J. Chem. Phys.* **2007**, *127*, 104105.
(11) Jansen, T. L. C.; Ruszel, W. M. *J. Chem. Phys.* **2008**, *128*, 214501.
(12) Yang, M.; Skinner, J. L. *J. Chem. Phys.* **2011**, *135*, 154114.
(13) Jansen, T. L. C.; Knoester, J. *J. Phys. Chem. B* **2006**, *110*, 22910.
(14) Torii, H. *J. Phys. Chem. A* **2006**, *110*, 4822.
(15) Jansen, T. L. C.; Knoester, J. *Biophys. J.* **2008**, *94*, 1818−1825.
(16) Paarmann, A.; Hayashi, T.; Mukamel, S.; Miller, R. J. D. *J. Chem. Phys.* **2009**, *130*, 204110.
(17) Falvo, C.; Palmieri, B.; Mukamel, S. *J. Chem. Phys.* **2009**, *130*, 184501.
(18) Jansen, T. L. C.; Auer, B. M.; Yang, M.; Skinner, J. L. *J. Chem. Phys.* **2010**, *132*, 224503.

(19) Jansen, T. L. C.; Hayashi, T.; Zhuang, W.; Mukamel, S. *J. Chem. Phys.* **2005**, *123*, 114504.
(20) Jansen, T. L. C.; Zhuang, W.; Mukamel, S. *J. Chem. Phys.* **2004**, *121*, 10577.
(21) Sanda, F.; Mukamel, S. *J. Chem. Phys.* **2006**, *125*, 014507.
(22) Kobus, M.; Gorbunov, R. D.; Nguyen, P. H.; Stock, G. *Chem. Phys.* **2008**, *347*, 208.
(23) Brüggeman, B.; Kjellberg, P.; Pullerits, T. *Chem. Phys. Lett.* **2007**, *444*, 192.
(24) Kjellberg, P.; Brüggeman, B.; Pullerits, T. *Phys. Rev. B* **2006**, *74*, 024303.
(25) Ishizaki, A.; Tanimura, Y. *J. Phys. Chem. A* **2007**, *111*, 9269.
(26) Kreisbeck, C.; Kramer, T.; Rodriguez, M.; Hein, B. *J. Chem. Theory Comput.* **2011**, *7*, 2166−2174.
(27) Heijs, D.; Dijkstra, A. G.; Knoester, J. *Chem. Phys.* **2007**, *341*, 230.
(28) Mukamel, S. *Principles of Nonlinear Optical Spectroscopy*; Oxford University Press: New York, 1995.
(29) Ishizaki, A.; Tanimura, Y. *J. Phys. Soc. Jpn.* **2005**, *74*, 3131.
(30) Hanna, G.; Geva, E. *J. Phys. Chem. B* **2009**, *113*, 9278−9288.
(31) McRobbie, P. L.; Hanna, G.; Shi, Q.; Geva, E. *Acc. Chem. Res.* **2009**, *42*, 1299−1309.
(32) Yagasaki, T.; Saito, S. *J. Chem. Phys.* **2008**, *128*, 154521.
(33) Jansen, T. L. C.; Snijders, J. G.; Duppen, K. *J. Chem. Phys.* **2000**, *113*, 307.
(34) Hasegawa, T.; Tanimura, Y. *J. Chem. Phys.* **2008**, *128*, 065411.
(35) Hamm, P.; Zanni, M. T. *Concepts and Methods of 2D Infrared Spectroscopy*; Cambridge University Press: Cambridge, U. K., 2011.
(36) Jansen, T. L. C.; Knoester, J. *Acc. Chem. Res.* **2009**, *42*, 1405−1411.
(37) Leforestier, C.; Bisseling, R. H.; Cerjan, C.; Feit, M. D.; Friesner, R.; Guldberg, A.; Hammerich, A.; Jolicard, G.; Karrlein, W.; Meyer, H. D.; Lipkin, N.; Roncero, O.; Kosloff, R. *J. Comput. Phys.* **1991**, *94*, 59−80.
(38) Lindahl, E.; Hess, B.; Spoel, D. v. d. *J. Mol. Model.* **2001**, *7*, 306.
(39) de Raedt, H. *Comput. Phys. Rep.* **1987**, *7*, 1−72.
(40) Kosloff, R. *J. Phys. Chem.* **1988**, *92*, 2087−2100.
(41) Kwac, K.; Lee, H.; Cho, M. *J. Chem. Phys.* **2004**, *120*, 1477.
(42) Hochstrasser, R. M. *Chem. Phys.* **2001**, *266*, 273−284.
(43) Jansen, T. L. C.; Knoester, J. *J. Chem. Phys.* **2006**, *124*, 044502.
(44) Liang, C.; Jansen, T. L. C.; Knoester, J. *J. Chem. Phys.* **2011**, *134*, 044502.
(45) Townsley, L. E.; Tucker, W.; Sham, S.; Hinton, S.; Hinton, J. *Biochem.* **2001**, *40*, 11676.
(46) Jansen, T. L. C.; Dijkstra, A. G.; Watson, T. M.; Hirst, J. D.; Knoester, J. *J. Chem. Phys.* **2006**, *125*, 044312.
(47) Burkhart, B.; Li, N.; Langs, D.; Pangborn, W.; Duax, W. *Proc. Natl. Acad. Sci. U. S. A.* **1998**, *95*, 12950.
(48) Abramavicius, D.; Palmieri, B.; Voronine, D.; Sanda, F.; Mukamel, S. *Chem. Rev.* **2009**, *109*, 2350−2408.
(49) Olbrich, C.; Jansen, T. L. C.; Liebers, J.; Aghtar, M.; Strümpfer, J.; Schulten, K.; Knoester, J.; Kleinekathöfer, U. *J. Phys. Chem. B* **2011**, *115*, 8609−8621.
(50) Jansen, T. L. C. NISE2A, 2012. This program is available for free on e-mail request.
(51) Humphrey, W.; Dalke, A.; Schulten, K. *J. Mol. Graphics* **1996**, *14*, 33−38.